Electronic Supplementary Material (ESI) for Soft Matter.

Supplemental information

Modeling of shape memory polymer sheets that self-fold in response to localized heating

Russell W. Mailen[a], Ying Liu[b], Michael D. Dickey[b,*], Mohammed Zikry [a,*], Jan Genzer [b,*]

[a.] *Department of Mechanical and Aerospace Engineering, NC State University. 911 Oval Drive, Raleigh, NC 27695, USA.*

[b.] *Department of Chemical and Biomolecular Engineering, NC State University, 911 Partners Way, Raleigh NC 27695, USA.*

Email: Michael_dickey@ncsu.edu, zikry@ncsu.edu, jan_genzer@ncsu.edu

Our model for the self-folding of pre-strained polymer sheets is based on the experimental procedure used in our previous publication.[1] A brief description of the procedure follows. First, pattern hinges on Shrinky-Dink sheets using a desktop inkjet printer. Then cut the samples to the desired size. Place the sample on a hotplate set to 90°C to bring the sample temperature close to the glass transition (T_g) of the polymer. After the temperature of the sample has stabilized, turn on an unfocused IR heat lamp located approximately 5 cm above the sample. Record the bending angle using a video camera and the hinge surface temperature using an IR camera.

The geometric model, develop previously, assumes that the top surface of the hinge shrinks completely during folding while the bottom does not shrink at all and that the axial shrinkage varies linearly through the depth of the hinge.[2] The geometric model also assumes that the thickness of the polymer does not increase during the folding process. This assumption does not account for mass conservation. **Figure S1a** offers a slightly modified version of the simple geometric model that accounts for both top and bottom surface shrinkage according to:

$$\alpha_b = 2\tan^{-1}\left(\frac{W}{2h}(S_1 - S_2)\right), \tag{S1}$$

where W is the width of the hinge on the pre-strained material, h is the thickness of the polymer sheet, and S_1 and S_2 are the shrinkage of the top and bottom surfaces of the hinged region, respectively. Shrinkage was defined previously in Equation 1. **Figure S1b** shows the results of this model for a sample with a 2 mm hinge width. The α_b is maximized when the top surface shrinks completely and the bottom surface does not shrink at all. However, experimental results published previously do not maximize α_b (maximum experimental bending angle $\alpha_{b,max} = 100°$ for a 2 mm hinge width).[2] The α_b is reduced by shrinking of the bottom of the hinge so that one α_b can be achieved by a combination of top and bottom surface shrinkage. If the bottom surface continues to shrink after the top has shrunk completely, the sample unfolds as seen experimentally.

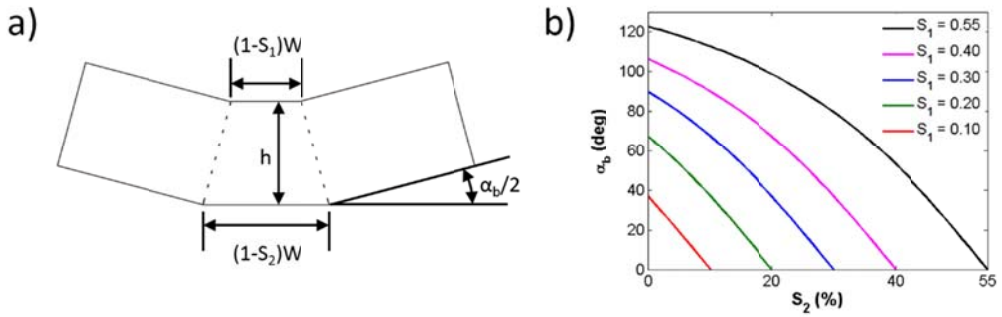

Figure S1. Alternate geometric model that accounts for shrinkage of top and bottom hinge surfaces. a) Geometric definitions. b) Bending angle (α_b) predicted by alternate geometric model for a range of top and bottom surface shrinkage values.

To model the shrinkage and folding behavior of the pre-strained polystyrene polymer sheet, we first evaluate the viscoelastic properties of the material. A TA Instruments AR2000 rheometer with a torsion-bar clamp fixture measured the time and temperature dependent shear modulus. Pre-shrunk samples were mounted in the fixture and subjected to an oscillatory strain of 0.2% across a frequency sweep from 0.03 Hz - 0.8 Hz. This frequency sweep was repeated at

5° increments ranging from 95 to 120°C. The reaction force was obtained as a function of strain and frequency, and the material shear storage modulus (G'), shear loss modulus (G''), and phase angle ($\tan(\delta) = G''/G'$) were calculated. **Figures 4a,c** in the paper plot the storage modulus and phase angle as measured by the rheometer, respectively. A vertical shift of T_g/T (temperatures in Kelvin) has been applied to the storage and loss modulus data used to obtain these plots. These curves can be shifted horizontally in frequency according to the time-temperature superposition principle to allow the evaluation of viscoelastic material properties at frequencies or temperatures that are otherwise not measurable. Once shifted, the isothermal curves make up a viscoelastic master curve at the selected reference temperature. Assuming that the material is thermo-rheologically simple, the isothermal curves can be shifted in frequency according to the Williams-Landel-Ferry (WLF) equation:[3]

$$\log(a_t) = -\frac{C_1(T - T_{ref})}{C_2 + (T - T_{ref})}, \tag{S2}$$

where C_1 and C_2 are empirical parameters, T is the experimental temperature, and T_{ref} is typically taken as the glass transition temperature, T_g. Reasonable alignment of the shear modulus curves was obtained with the standard WLF shift factors of $C_1 = 17.44$ and $C_2 = 51.6$ [3] and a reference temperature of $T_{ref} = T_g = 103$°C. After obtaining the master curve, the time-temperature dependent behavior at any temperature above the glass transition temperature T_g can be determined through further application of the time-temperature superposition principle.

The viscoelastic master curve obtained by the time-temperature superposition principle can be modeled using a Prony series to represent a generalized Maxwell model[4,5]. To do this, a series of suitable dimensionless relaxation moduli g_i and relaxation times τ_i were calculated to fit a Prony series to G' and G'' using a bounded search algorithm implemented in Matlab. The Prony series for the storage and loss moduli of a viscoelastic material can be implemented in ABAQUS[5] according to:

$$G'(f) = G_0\left[1 - \sum_{i=1}^{n} g_i\right] + G_0 \sum_{i=1}^{n} \frac{g_i (2\pi f \tau_i)^2}{1 + (2\pi f \tau_i)^2}, \tag{S3}$$

$$G''(f) = G_0 \sum_{i=1}^{n} \frac{g_i (2\pi f \tau_i)}{1 + (2\pi f \tau_i)^2}, \tag{S4}$$

where G_0 is the instantaneous shear modulus and f is the frequency in Hz. The generalized Maxwell model is validated by the fit of the model to the experimental storage modulus data (*cf.* **Figure 4b**), and the model is further validated by the fit of the model to the phase angle data as shown in **Figure 4d**. As seen in these plots, the fit of the model begins to deteriorate as the material enters the rubbery plateau and terminal zones of the data (low frequency). This is attributed to the fact that polystyrene is a thermoplastic that will flow at higher temperatures or low frequencies (long times) even though the molecular weight of Shrinky-Dinks exceeds the entanglement molecular weight of polystyrene. The calculated Prony series coefficients are summarized in **Table I**. Other material properties used as inputs to the finite element model are listed in **Table II**.

Table I. Prony series coefficients for Shrinky-Dink material

#	1	2	3	4	5	6
g_i	0.2089	0.3654	0.3037	0.1011	0.01243	0.004661
τ_i (s)	1.182	14.77	114.8	402	3096	25680

Table II. Material properties used in the finite element model

Property	Value	Reference
Thermo-Rheologically Simple WLF Parameters	$C_1 = 17.44$	[3]
	$C_2 = 51.6$	[3]
	$T_{ref} = T_g = 103°C$	this work
Instantaneous Elastic Modulus, E	1.78×10^9 *Pa*	this work
Poisson's Ratio, v	0.33 ($T < T_g$)	[6]
	0.4995 ($T > T_g$)	
Thermal Conductivity, k	0.14 *W/mK*	[7]
Density, ρ	1050 kg/m^3	[8]
Thermal Expansion	2.09×10^{-4} K^{-1} ($T < T_g$)	[6]
	5.65×10^{-4} K^{-1} ($T > T_g$)	[6]
Specific Heat	1300 *J/kgK*	this work

The in-plane shrinkage model makes use of two planes of symmetry (*cf.* **Figure S2c**). The dimensions of the model prior to shrinking were 10 mm (length) × 10 mm (width) × 0.3 mm (thickness). Following the pre-straining sequence, the model was subjected to a specified temperature boundary condition on all surfaces that were not planes of symmetry as shown in **Figure S2b**. Mechanical displacement normal to each plane of symmetry was prevented in addition to a prevention of out-of-plane (Z-direction) displacement of one node at the intersection of the two planes of symmetry.

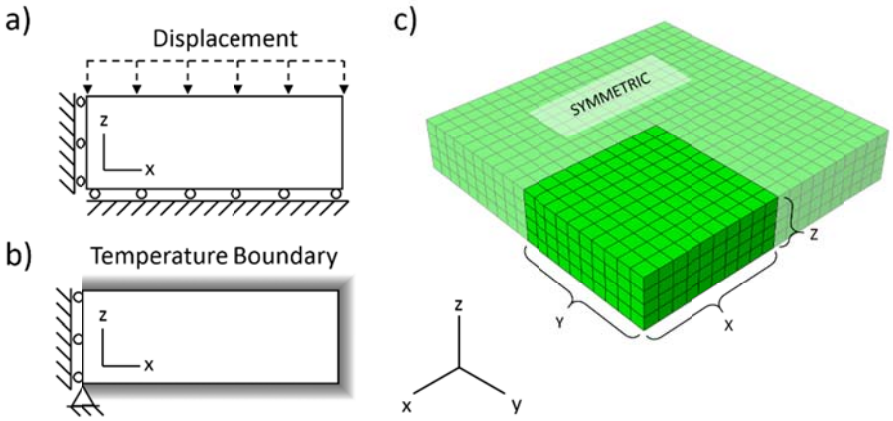

Figure S2. In-plane shrinkage model. a) Mechanical boundary conditions during programming sequence. b) Mechanical and thermal boundary condition of in-plane shrinkage model during shrinking process. c) In-plane folding model showing model symmetry and mesh. Labels specify the number of elements that span the indicated region. X=10 elements. Y=10 elements. Z=4 elements.

We evaluate the effect that cooling rate during material prestraining has on the Shrinky-Dink material recovery. Increasing the time to cool the sample (*i.e.*, a lower cooling rate) reduced the initial rate of recovery of the sample as seen in **Figure S3**. This effect is most noticeable for isothermal recovery near T_g. In the comparison of recovery model results to experimental data, the experimental process of placing the sample in the hot stage which then must re-establish the preset temperature then taking the sample out of the hot stage for measurement introduces uncertainty, which has not been quantified and may account for some of the discrepancies in the comparisons. Additionally, although the samples nominally shrink ~55% in both in-plane directions, this value may vary by a few percent from sample to sample as well with some variation within each sample.

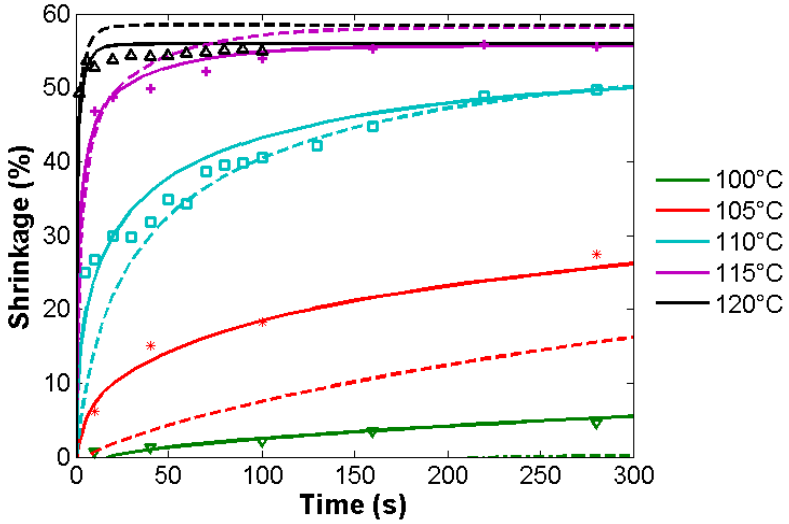

Figure S3. Comparison of effect of short and long cooling times on isothermal recovery behavior. Samples programmed by short cooling time shown as solid lines. Samples programmed by long cooling time are shown as dashed lines. Experimental data are shown as symbols.

The out-of-plane folding model with one plane of symmetry was shown in **Figure 2**. Following the pre-straining sequence, the model was subjected to convective boundary conditions on all surfaces that were not the plane of symmetry. An additional thermal boundary condition was applied to the hinge surface to model heating of the hinge surface. Mechanical displacement normal to the plane of symmetry was prevented in addition to fixed displacements at specific locations on the model as shown in **Figure 2b**. Initially, a model for the folding of a sample with a 1 mm hinge width was developed. To account for the non-uniform thermal boundary conditions, a convective heat transfer coefficient of $h = 5$ *W/mK* and sink temperature of 90°C was applied to all surfaces except the face in contact with the hot plate and the back of the hinge. For the face in contact with the hot plate, a convective heat transfer coefficient of $h = 2000$ *W/mK* and sink temperature of 90°C was applied to model the thermal contact conductance between the hot plate and the polymer. For the back of the hinge, which lifts away from the hot plate through the folding process, a heat transfer coefficient that transitions from $h =$ 2000 *W/mK* to $h = 5$ *W/mK* across the width of the hinge was applied. These thermal boundary conditions were validated by applying the experimentally measured hinge temperature to the hinge region of the model. The model results provide a very reasonable comparison of bending angle to the experimental results as seen in **Figure S4**. For the larger hinge widths, the same length of transition for the heat transfer coefficient on the back side of the hinge as that for the 1 mm hinge width model was used, although the location of this transition on the back of the hinge was shifted toward the edge of the hinge nearest the hot-plate.

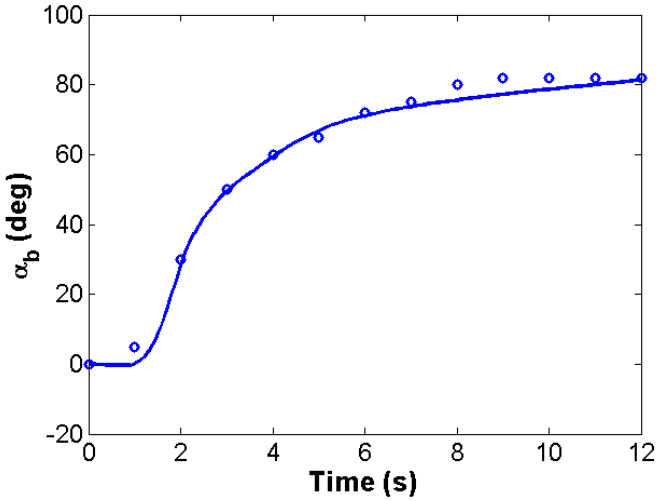

Figure S4. Bending angle results obtained by specifying experimentally measured hinge temperature for 1 mm hinge width model. The solid line represents model results. Symbols represent experimental results.

A suitable model for the IR heat flux was developed based on reported values for the IR heat flux measured by a thermopile and comparison of modeled temperature results to the measured hinge temperature. The IR flux of the light in the experimental setup is ~1,000 mW/cm^2 (=10,000 W/m^2);[1] this value was initially applied as a constant heat flux on the hinge surface. A model of the 1 mm hinge width sample using this constant surface heat flux underpredicts the maximum bending angle of the hinge. Additionally, the average temperature of the hinge heated by a surface heat flux (because the temperature is non-uniform when heated by a surface heat flux) is

lower than the experimentally measured temperature. This experimentally measured temperature is somewhat misleading because the software for the IR camera smooths the experimental data, and the IR image is pixelated due to necessary aspects of the experimental setup. Because the bending angle and temperature were underpredicted, a range of constant surface heat flux values were evaluated. As seen in **Figure S5**, no single, constant surface heat flux accurately reproduced the bending angle and average hinge temperature. Instead, a non-constant heat flux was used that rapidly increases when the light is turned on and eventually approaches some constant value. This heat flux variation is representative of the mechanism of light production in an IR light where electrical current flowing through the filament in the lightbulb initially causes a rapid heating of the filament, and after a while, the filament approaches a constant temperature that yields a constant heat flux. The time to reach constant heat flux is long compared to the duration of the experiment.

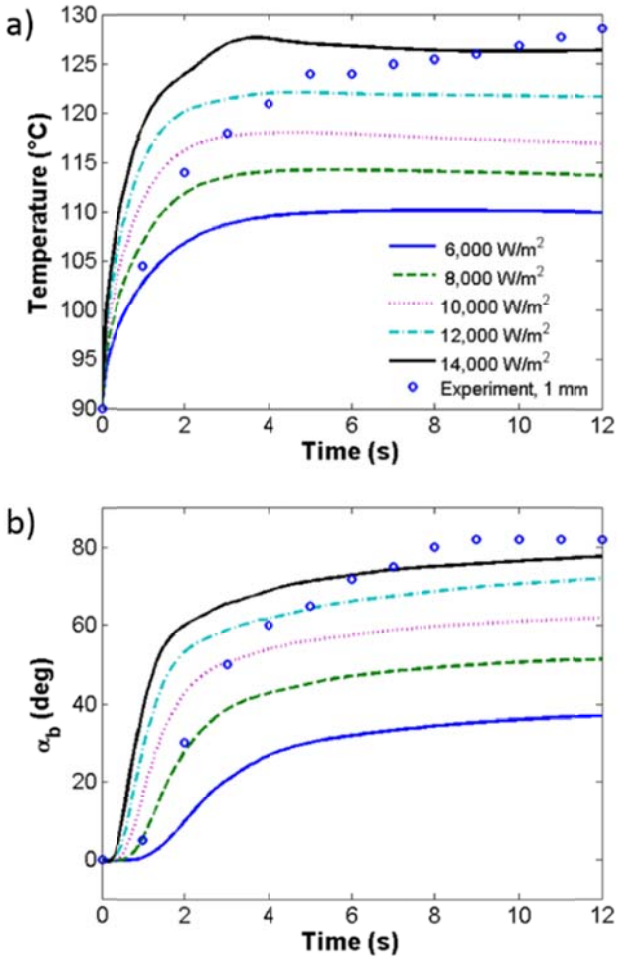

Figure S5. Constant IR flux results for 1 mm hinge. a) Average hinge temperature results. b) Bending angle results. Solid lines represent model results. The symbols represent experimental results.

The local, axial shrinkage field in **Figure 8a** was calculated by determining the shrinkage between two adjacent nodes in the model, and then assigning that shrinkage to the midpoint between those nodes. This axial shrinkage field moves and rotates with the hinge locally as it

folds. Additionally, information for the shrinkage profile through the thickness along the folding angle bisection line was extracted from the model by first selecting two nodes each on the top and bottom of the lifted and non-lifted face of the folding polymer away from the hinged region (8 nodes total). The two intersection points of vectors defined by these sets of nodes are used to define the folding angle bisection vector. These vectors are depicted as gray lines in **Figure 8a**.

References

1 Y. Liu, J.K. Boyles, J. Genzer, M.D. Dickey, *Soft Matter*, 2012, **8**, 1764–1769.

2 Y. Liu, R. Mailen, Y. Zhu, M.D. Dickey, J. Genzer, *Phys. Rev. E*, 2014, **89**, 042601.

3 M.L. Williams, R.F. Landel, J.D. Ferry, *J. Am. Chem. Soc.*, 1955, **77**, 3701–3707.

4 H.F. Brinson, *Polymer engineering science and viscoelasticity : an introduction*, Springer, New York, 2008.

5 Analysis User's Manual 6.12. ABAQUS. Dassault Systèmes.

6 *Polymer handbook* (J. Brandrup, E.H. Immergut, E.A. Grulke, Editors), Wiley-Interscience, New York, 1999.

7 N. Demarse, TA Instruments, personal communication, 2013.

8 G. Natta, *J. Polym. Sci.*, 1955, **16**, 143–154.